Article

Template Adaptability Is Key in the Oriented Crystallization of CaCO

Daniela C. Popescu, Maarten M. J. Smulders, Benot P. Pichon, Natalia Chebotareva, Seo-Young Kwak, Otto L. J. van Asselen, Rint P. Sijbesma, Elaine DiMasi, and Nico A. J. M. Sommerdijk

J. Am. Chem. Soc., **2007**, 129 (45), 14058-14067• DOI: 10.1021/ja075875t • Publication Date (Web): 18 October 2007

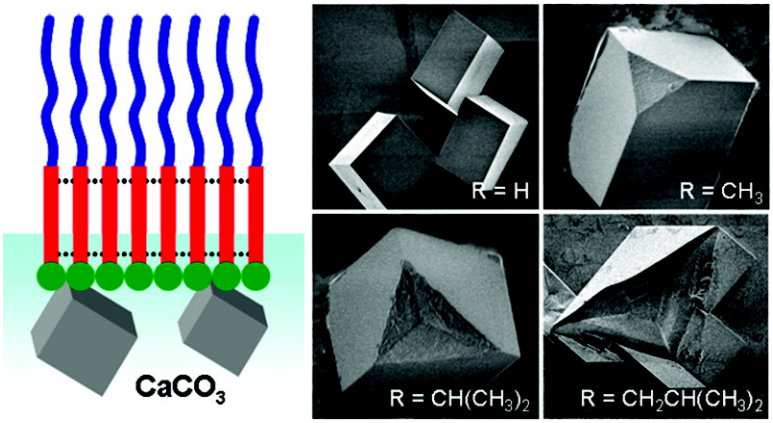

More About This Article

Additional resources and features associated with this article are available within the HTML version:

- Supporting Information
- Links to the 9 articles that cite this article, as of the time of this article download
- Access to high resolution figures
- Links to articles and content related to this article
- Copyright permission to reproduce figures and/or text from this article

View the Full Text HTML

J|A|C|S
ARTICLES
Published on Web 10/18/2007

Template Adaptability Is Key in the Oriented Crystallization of $CaCO_3$

Daniela C. Popescu,[†] Maarten M. J. Smulders,[†] Benoît P. Pichon,[†] Natalia Chebotareva,[†] Seo-Young Kwak,[‡] Otto L. J. van Asselen,[§] Rint P. Sijbesma,[†] Elaine DiMasi,*[,‡] and Nico A. J. M. Sommerdijk*[,†,||]

Contribution from the Laboratory for Macromolecular and Organic Chemistry, Eindhoven University of Technology, Eindhoven, The Netherlands, National Synchrotron Light Source, Brookhaven National Laboratory, Upton, New York 11973, Laboratory of Polymer Technology, Eindhoven University of Technology, Eindhoven, The Netherlands, and Soft Matter CryoTEM Research Unit, Eindhoven University of Technology, Eindhoven, The Netherlands

Received August 6, 2007; E-mail: N.Sommerdijk@tue.nl; dimasi@bnl.gov

Abstract: In $CaCO_3$, biomineralization nucleation and growth of the crystals are related to the presence of carboxylate-rich proteins within a macromolecular matrix, often with organized β-sheet domains. To understand the interplay between the organic template and the mineral crystal it is important to explicitly address the issue of *structural adaptation* of the template during mineralization. To this end we have developed a series of self-organizing surfactants (**1**−**4**) consisting of a dodecyl chain connected via a bisureido-heptylene unit to an amino acid head group. In Langmuir monolayers the spacing of these molecules in one direction is predetermined by the hydrogen-bonding distances between the bis-urea units. In the other direction, the intermolecular distance is determined by steric interactions introduced by the side groups (−R) of the amino acid moiety. Thus, by the choice of the amino acid we can systematically alter the density of the surfactant molecules in a monolayer and their ability to respond to the presence of calcium ions. The monolayer films are characterized by surface pressure−surface area (π−A) isotherms, Brewster angle microscopy, in-situ synchrotron X-ray scattering at fixed surface area, and also infrared reflection absorption spectroscopy (IRRAS) of films transferred to solid substrates. The developing crystals are studied with scanning and transmission electron microscopy (SEM, TEM), selected area electron diffraction (SAED), and crystal modeling. The results demonstrate that although all compounds are active in the nucleation of calcium carbonate, habit modification is only observed when the size of the side group allows the molecules to rearrange and adapt their organization in response to the mineral phase.

Introduction

The study of biomineralization has a long history, beginning with observations of these uniquely biogenic structures and now manifesting itself in intense scrutiny of the organic macromolecules which control the underlying mineralization processes.[1−3] The current emphasis on determining the principal biomineralization mechanisms in calcium carbonates has led to several important insights. It was observed that $CaCO_3$ nucleation and growth are related to the presence of carboxylate (e.g., aspartate- and glutamate-rich) proteins within the macromolecular matrix, often with organized β-sheet domains.[2,4−6] The concept that the structural organization of the organic matrix was crucial for biomineral templating motivated many studies to explore peptides and macromolecules with predefined secondary structures.[6−16] The preparation of organized functional molecules

[†] Laboratory for Macromolecular and Organic Chemistry, Eindhoven University of Technology.
[‡] Brookhaven National Laboratory.
[§] Laboratory of Polymer Technology, Eindhoven University of Technology.
[||] Soft Matter CryoTEM Research Unit, Eindhoven University of Technology.

(1) Harting, P. Q. *J. Microsc. Sci.* **1872**, *12*, 118−123.
(2) Mann, S. *Biomineralization. Principles and Concepts in Bioinorganic Materials Chemistry*; Oxford University Press: New York, 2001.
(3) Li, C.; Kaplan, D. L. *Curr. Opin. in Solid State and Materials Sci.* **2003**, *7*, 265−271.
(4) Weiner, S.; Hood, L. *Science* **1975**, *190*, 987−989.
(5) Levi-Kalisman, Y.; Falini, G.; Addadi, L.; Weiner, S. *J. Struct. Biol.* **2001**, *135*, 8−17.
(6) Meldrum, F. C. *Int. Mater. Rev.* **2003**, *48*, 187−224.
(7) Falini, G.; Weiner, S.; Addadi, L. *Cal. Tissue Int.* **2003**, *72*, 548−554.
(8) Addadi, L.; Moradian, J.; Shay, E.; Maroudas, N. G.; Weiner, S. *Proc. Natl. Acad. Sci. U.S.A.* **1987**, *84*, 2732−2736.
(9) Subburaman, K.; Pernodet, N.; Kwak, S. Y.; DiMasi, E.; Ge, S.; Zaitsev, V.; Ba, X.; Yang, N. L.; Rafailovich, M. *Proc. Natl. Acad. Sci. U.S.A.* **2006**, *103*, 14672−14677.
(10) Addadi, L.; Moradian-Oldak, J.; Weiner, S. *Macromolecule-Crystal Recognition in Biomineralization*. In *Surface Reactive Peptides and Polymers*; Sikes, C. S., Wheeler, A. P., Eds.; ACS Symposium Series Vol. 444; American Chemical Society: Washington, DC, 1991; pp 13−27.
(11) DeOliveira, D. B.; Laursen, R. A. *J. Am. Chem. Soc.* **1997**, *119*, 10627−10631.
(12) Falini, G.; Fermani, S.; Gazzano, M.; Ripamonti, A. *J. Chem. Soc., Dalton Trans.* **2000**, 3983−3987.
(13) Levi, Y.; Albeck, S.; Brack, A.; Weiner, S.; Addadi, L. *Chem.—Eur. J.* **1998**, *4*, 389−396.
(14) Donners, J. J. J. M.; Nolte, R. J. M.; Sommerdijk, N. A. J. M. *J. Am. Chem. Soc.* **2002**, *124*, 9700−9701.
(15) D'Souza, S. M.; Alexander, C.; Carr, S. W.; Waller, A. M.; Whitcombe, M. J.; Vulfson, E. N. *Nature* **1999**, *398*, 312−316.
(16) Meegan, J. E.; Aggeli, A.; Boden, N.; Brydson, R.; Brown, A. P.; Carrick, L.; Brough, A. R.; Hussain, A.; Ansell, R. J. *Adv. Funct. Mater.* **2004**, *14*, 31−37.

10.1021/ja075875t CCC: $37.00

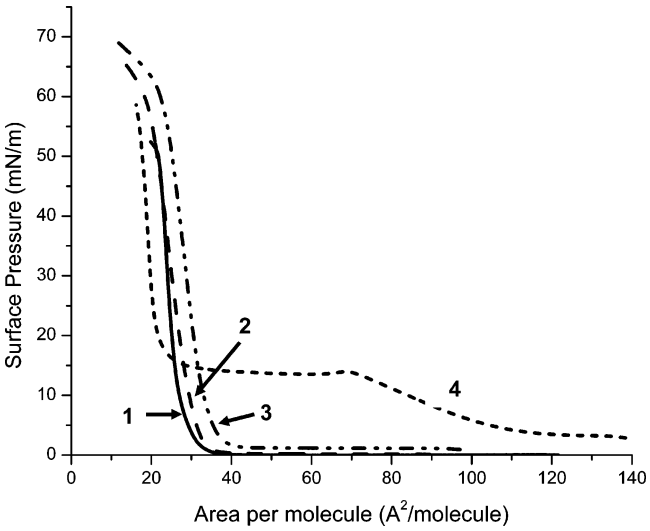

Figure 1. Langmuir isotherms of **1**−**4** recorded on water at 20 °C.

at interfaces made it possible to create *in vitro* experiments focusing on very specific aspects of the mineral−organic interface. Systems studied included compressed[17] and self-organized Langmuir monolayers,[18−21] polymerized films,[22] self-assembled alkanethiol monolayers,[23−25] and functionalized gold colloids.[24,26] More recently also the influence of a gel present at the nucleation interface was described.[27]

Originally many authors have searched for an epitaxial relation between template and mineral to explain observations of oriented nucleation.[17,28] More recently additional mechanisms such as orientational complementarity of functional groups[14,23,25] and the role of electrostatic interactions[29] have been promoted. In retrospect the concept of organic−mineral epitaxy, although confirmed by in situ scattering experiments in a BaF_2−fatty acid model system,[30] demands a difficult circumstance in that a relatively soft macromolecular assembly would remain rigid enough to drive nucleation of a preferred crystal face whose lattice parameters are rather immutable. By contrast it is known that proteins,[31] fatty acid films,[32] and possibly also collagenous tissue matrices[33] do rearrange their structures upon exposure to mineral ions.

Table 1. Wavenumbers of the N−H, C═O, and Amide II Vibration Bands in the FTIR Spectra of **1**−**4**

	dropcast film			monolayer
amphiphile	N−H stretching (cm^{-1})	C═O stretching (cm^{-1})	amide II (cm^{-1})	amide II[a] (cm^{-1})
1	3331	1611	1585	1582
2	3331	1611	1585	1576
3	3337	1613	1574	1575
4	3336	1613	1571	nd

[a] From IRRAS; nd = not determined (see ref 36).

To understand the interplay between the organic template and the mineral crystal it is important to explicitly address the issue of *structural adaptation* of the template during mineralization. To address this question, we have developed a series of self-organizing surfactants (**1**−**4**) consisting of a dodecyl chain connected via a bisureido-heptylene unit to an amino acid head group. In Langmuir monolayers the spacing of these molecules

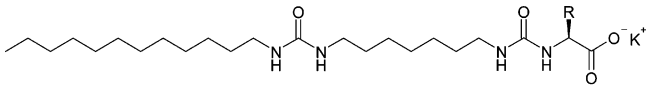

1: R=H, **2**: R=CH_3, **3**: R=$CH(CH_3)_2$, **4**: R=CH_2 $CH(CH_3)_2$

in one direction is expected to be predetermined by the hydrogen-bonding distances between the bis-urea units. In the other direction, the intermolecular distance will be determined by steric interactions introduced by the side groups (−R) of the amino acid moiety. This system for the first time allows us to modulate the molecular packing and the concomitant flexibility of the monolayer in a systematic way. In this paper we will demonstrate that although all compounds are active in the nucleation of calcium carbonate, habit modification is only observed when the size of the side group allows the molecules to rearrange and adapt their organization in response to the mineral phase.

Materials and Methods

Langmuir Film Experiments. All the isotherms were recorded in an integrated dust-free cabinet at 20 °C and ambient humidity. Monolayers were formed by spreading solutions of **1** (0.5 mg/mL) from $CHCl_3/CH_3OH$/TFA (4/1/0.05, v/v/v) and **2** (0.5 mg/mL), **3** (1 mg/mL), and **4** (1 mg/mL) from $CHCl_3/CH_3OH$ (4/1, v/v) on water, aqueous 9 mM $CaCl_2$, or supersaturated $Ca(HCO_3)_2$ subphases in a commercial Teflon Langmuir trough (KSV Minitrough, KSV Instrument Ltd., Helsinki, Finland). The monolayer was left undisturbed for 15 min to allow solvent evaporation prior to compression. Computer controlled symmetrically movable hydrophobic Delrin (polyacetal) barriers were used to regulate the surface area. The trough dimensions were 260 mm × 75 mm × 5 mm. The surface pressure was measured by a Pt Wilhelmy plate with a sensitivity of ±0.01 mN/m. The clean subphase was taken as the surface pressure zero reference. The compression rate was set at 5 mm/min.

Charge Density Determination. The charge densities of the monolayers of **1** (3.7 $e^-\cdot nm^{-2}$) and **3** (3.7 $e^-\cdot nm^{-2}$) were calculated from the limiting mean molecular areas on a subphase containing 9 mM $Ca(HCO_3)_2$ (obtained by extrapolation of the slope of the curve to zero pressure) and expressed as the amount of charged groups per nm^2.

(17) Mann, S.; Heywood, B. R.; Rajam, S.; Birchall, J. D. *Nature* **1988**, *334*, 692−695.
(18) Buijnsters, P. J. J. A.; Donners, J. J. J. M.; Hill, S. J.; Heywood, B. R.; Nolte, R. J. M.; Zwanenburg, B.; Sommerdijk, N. A. J. M. *Langmuir* **2001**, *17*, 3623−3628.
(19) Champ, S.; Dickinson, J. A.; Fallon, P. S.; Heywood, B. R.; Mascal, M. *Angew. Chem., Int. Ed.* **2000**, *39*, 2716−2719.
(20) Lahiri, J.; Xu, G.; Dabbs, D. M.; Yao, N.; Aksay, I. A.; Groves, J. T. *J. Am. Chem. Soc.* **1997**, *119*, 5449−5450.
(21) Cavalli, S.; Popescu, D. C.; Tellers, E. E.; Vos, M. R. J.; Pichon, B. P.; Overhand, M.; Rapaport, H.; Sommerdijk, N. A. J. M.; Kros, A. *Angew. Chem., Int. Ed.* **2006**, *45*, 739−744.
(22) Berman, A.; Ahn, D. J.; Lio, A.; Salmeron, M.; Reichert, A.; Charych, D. *Science* **1995**, *269*, 515−518.
(23) Aizenberg, J.; Black, A. J.; Whitesides, G. M. *J. Am. Chem. Soc.* **1999**, *121*, 4500−4509.
(24) Kuther, J.; Seshadri, R.; Nelles, G.; Assenmacher, W.; Butt, H. J.; Mader, W.; Tremel, W. *Chem. Mater.* **1999**, *11*, 1317−1325.
(25) Travaille, A. M.; Donners, J. J. J. M.; Gerritsen, J. W.; Sommerdijk, N. A. J. M.; Nolte, R. J. M.; Kempen, H. v. *Adv. Mater.* **2002**, *14*, 492−495.
(26) Küther, J.; Seshadri, R.; Tremel, W. *Angew. Chem., Int. Ed.* **1998**, *37*, 3044−3047.
(27) Li, H. Y.; Estroff, L. A. *J. Am. Chem. Soc.* **2007**, *129*, 5480−5483.
(28) Heywood, B. R.; Rajam, S.; Mann, S. *J. Chem. Soc., Faraday Trans.* **1991**, *87*, 735−743.
(29) Volkmer, D.; Fricke, M.; Agena, C.; Mattay, J. *J. Mater. Chem.* **2004**, *14*, 2249−2259.
(30) Kmetko, J.; Yu, C.; Evmenenko, G.; Kewalramani, S.; Dutta, P. *Phys. Rev. Lett.* **2002**, *89*, 186102−186105.
(31) Nielbo, S.; Thomsen, J. K.; Graversen, J. H.; Jensen, P. H.; Etzerodt, M.; Poulsen, F. M.; Thogersen, H. C. *Biochemistry* **2004**, *43*, 8636−8643.
(32) DiMasi, E.; Olszta, M. J.; Patel, V. M.; Gower, L. B. *CrystEngComm* **2003**, *5*, 346−350.
(33) Beniash, E.; Traub, W.; Veis, A.; Weiner, S. *J. Struct. Biol.* **2000**, *132*, 212−225.

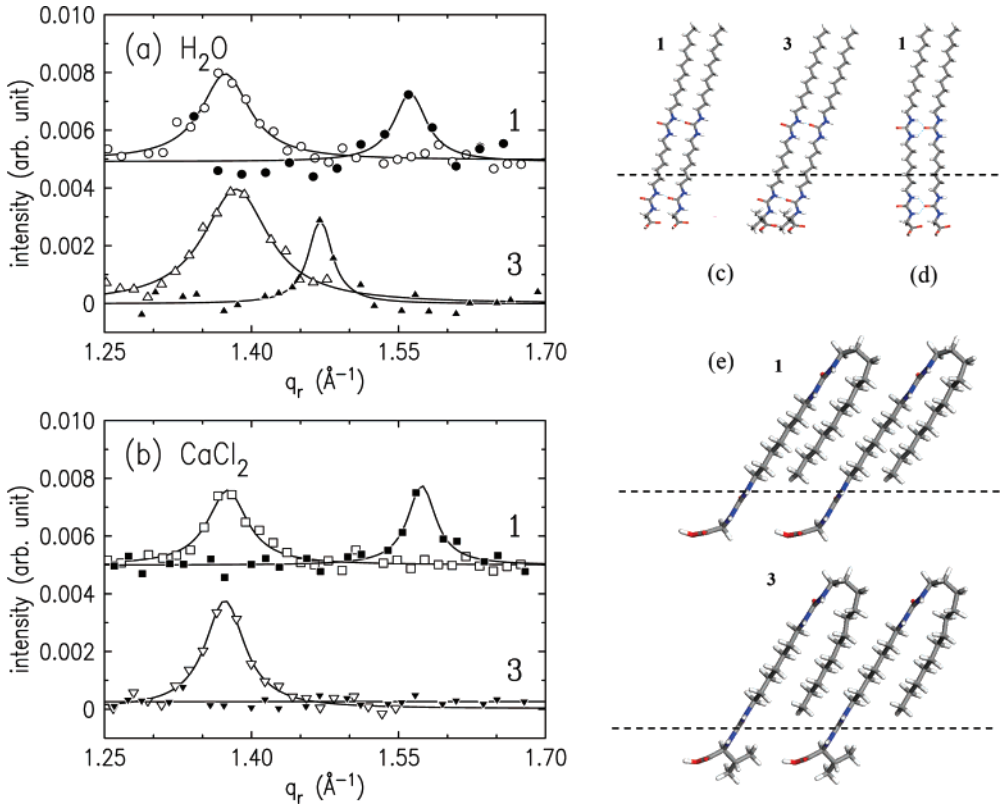

Figure 2. Background-subtracted X-ray diffraction peaks in grazing-incidence geometry as function of in-plane momentum transfer q_r for compounds **1** and **3** on (a) H_2O and (b) 9 mM $CaCl_2$ subphases. ○: **1**, q_z integrated over range with center = 0.3 Å^{-1}. ●: **1**, q_z = 0.9 Å^{-1}. △: **3**, q_z = 0.4 Å^{-1}. ▲: **3**, q_z = 0.75 Å^{-1}. □: **1**, q_z = 0.3 Å^{-1}. ■: **1**, q_z = 0.75 Å^{-1}. ▽: **3**, q_z = 0.4 Å^{-1}. ▼: **3**, no second peak observed. (c−e) Molecular models of **1** and **3**, dotted lines are drawn parallel to the air−water interface. (c) Stretched out molecules showing 12.3° and 17.3° tilts along H-bond direction. (d) Compound **1** with only the alkyl tail tilted. (e) Likely structures of **1** and **3** in Langmuir monolayers, with folded tails and tilts in both directions. In this configuration the H-bonds are perpendicular to the plane of the paper.

Literature values quoted for other systems producing [10.0] oriented calcite were calculated from the isotherms of **5** (2.0 e$^-$·nm^{-2}) and **6** (1.8 e$^-$·nm^{-2}) (see text) on aqueous subphases containing 9 mM $Ca(HCO_3)_2$ and 9 mM $CaCl_2$, respectively. For **6** the monoprotonated form was proposed as the one active in the mineralization reaction.

Infrared Spectroscopy and Infrared-Reflection Absorption Spectroscopy (IRRAS). Measurements were performed on monolayer films deposited on gold covered glass substrates. The molecules were compressed to a surface pressure of 40 mN/m and transferred to substrates by the Langmuir−Schaefer technique. A Biorad FTS6000 FTIR spectrometer, equipped with a DTGS detector, was used. The spectra were recorded with a resolution of 4 cm^{-1} and co-adding 1500 scans. For the reflection measurements (IRRAS) a Harrick Seagul accessory was used. The reflection angle was 80°. *P*-polarized radiation was obtained using a rotable wire grid polarizer. Transmission spectra were obtained from samples cast on a ZnSe window from the $CHCl_3$/CH_3OH solutions used for the Langmuir monolayer experiments.

Grazing Incidence X-ray Diffraction. In situ X-ray scattering measurements utilized the Harvard/BNL liquid surface spectrometer at beamline X22B, National Synchrotron Light Source, Brookhaven National Laboratory, using X-ray wavelength 1.53 Å and a Langmuir trough with a helium environment as described previously.[34] Grazing-incidence diffraction was conducted using a 0.12° incident angle, soller slit collimation with a 0.24° acceptance angle, and a vertically oriented position-sensitive detector with a 10 cm length. Reflectivity measurements used slit collimation and a scintillator detector.

The reflectivity was modeled by defining a surface-normal electron density profile rho(z) built of three error-function terms representing the subphase and the molecular film region. The model reflectivity is calculated in the kinetic approximation and fit to the data as described therein.[34] Note that the electron density which defines the scattered X-ray intensity arises from all electrons in the molecule and is not related to an uncompensated surface charge density which would arise from deprotonation of head groups or other binding and screening processes.

Mineralization Experiment. For all crystallization experiments an ~9 mM supersaturated solution of calcium bicarbonate ($Ca(HCO_3)_2$) prepared following the so-called Kitano method[35] was used. The solution was made by bubbling CO_2 gas through a suspension of $CaCO_3$ (3.5−4 g) in 1.5 L of ultrapure water (18 MΩ·cm) for 1.5 h, followed by filtration and CO_2 bubbling for another 30 min to dissolve any $CaCO_3$ particles present. Monomolecular films of **1**−**4** were spread from $CHCl_3$/CH_3OH/TFA or $CHCl_3$/CH_3OH solutions, at the air/water interface of freshly prepared supersaturated $Ca(HCO_3)_2$ solution poured in crystallization dishes (Schott Duran, Germany) (50 mL/dish) or in the Teflon Langmuir trough described above. For the crystallization dishes, the amount of molecules to spread was calculated taking into account the mean molecular areas found at π = 40 mN/m on the water subphase such that the molecules would cover 100% of the surface of the crystallization dish. For the experiments performed in the Langmuir trough, the monolayers were compressed until reaching the surface pressure π = 40 mN/m, which was maintained constant throughout the experiment.

Scanning Electron Microscopy (SEM). Crystals used for SEM investigation were collected from both the Langmuir trough and the crystallization dishes on glass microscopy slides (diameter = 15 mm, Menzel−Glasser, Germany) by vertical (Langmuir−Blodgett) and

(34) DiMasi, E.; Patel, V. M.; Sivakumar, M.; Olszta, M. J.; Yang, Y. P.; Gower, L. B. *Langmuir* **2002**, *18*, 8902−8909.

(35) Kitano, Y.; Park, K.; Hood, D. W. *J. Geophys. Res.* **1963**, *67*, 4873−4874.

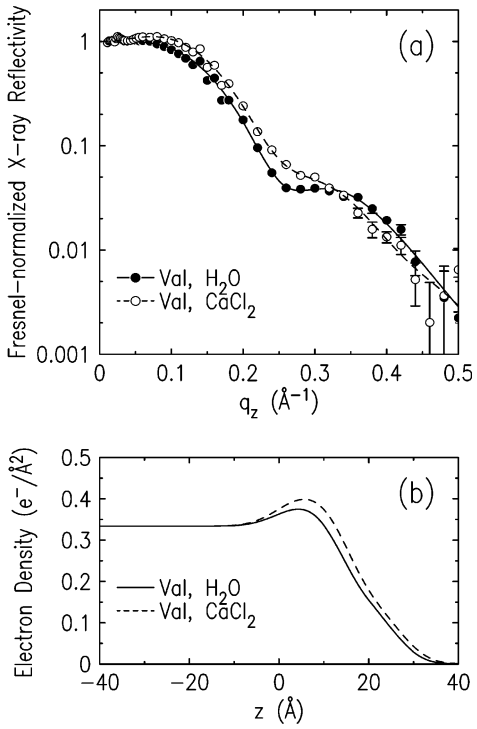

Figure 3. (a) Fresnel-normalized X-ray reflectivity from compound **3** on water (●) and 9 mM $CaCl_2$ (○). (b) Model electron density profiles from free two-slab fits to the data: (—) water, (- - -) $CaCl_2$.

horizontal (Langmuir−Schaefer) transfer after 4 h, following established procedures.[7] The samples were mounted on aluminum stubs with double-sided carbon tape. The specimens were observed with a Philips XL30 scanning electron microscope, using a secondary electron detector at an accelerating voltage of 1.0−2.0 kV.

Transmission Electron Microscopy (TEM). TEM was performed on a JEOL 2000-FX electron microscope operating at an accelerating voltage of 80 or 120 kV. Crystals used for selected area electron diffraction were collected from the crystallization dishes within 15 min after the start of the experiment by Langmuir−Schaefer transfer on carbon-coated TEM grids.

Results and Discussion

Self-Organization in Langmuir Monolayer. The self-organizing properties of the surfactant compounds were confirmed in Langmuir monolayers by surface pressure−surface area (π−A) isotherms, Brewster angle microscopy, in situ synchrotron X-ray scattering at fixed surface area, and also infrared reflection absorption spectroscopy (IRRAS) of films transferred to solid substrates.

Langmuir isotherms recorded on water (Figure 1) for compounds **1**−**3** are characterized by an increased lift-off area corresponding to an increasing volume of the side group. The limiting mean molecular area (MMA), determined from extrapolation of the slope in the condensed phase to zero surface pressure, increases from 27 Å^2 to 30 Å^2 to 34 Å^2 for **1**−**3**, respectively, demonstrating the effect of the larger head group in determining molecular spacing. By contrast the isotherm of compound **4**, the leucine derivative, showed a much higher lift-off area and upon further compression a plateau leading to a condensed phase of smaller limiting mean molecular area of 22 Å^2/molecule. Based on molecular models this area is too small for the nominal surface coverage, and it is apparent that the film was destabilized by excessive surface pressure, possibly collapsing into a partial bi- or multilayer. Thus compound **4** represents a regime where the large head group prevents the optimal self-organization exhibited by compounds **1**−**3**. Additional information was obtained for compound **2** using Brewster angle microscopy, in which separate mm-scale domains could be imaged even at $\pi = 0$ mN/m. Application of surface pressure simply pushed these domains into one continuous film with no change in image contrast, confirming the self-organizing nature of the films.

We predicted that the primary driver for self-organization would be the hydrogen bonding between bis-urea units. To investigate this, IRRA spectra were measured from compressed monolayers which were transferred to gold-coated glass substrates using the Langmuir−Schaefer technique. The spectra were compared to FT-IR transmission spectra of drop-cast films (Table 1).[36] The drop-cast samples showed N−H stretch, amide I, and amide II vibrations indicating strong hydrogen bonding, and only a small decrease in the hydrogen-bonding strength (as judged from the position of the amide II vibration) was observed going from **1**−**4** (Table 1). As IRRAS is only sensitive to vibrations that have a component oriented perpendicular to the substrate surface, the absence of the N−H and amide I vibrations in the spectra of the transferred monolayer indicated that in the monolayer of this compound the hydrogen bonds between the bis-urea units are oriented parallel to the film interface.[37] The presence of strong hydrogen bonds in the monolayer was confirmed by the position of the amide II bands.[38]

Quantitative information about intermolecular spacing was determined from in situ synchrotron X-ray diffraction, performed on Langmuir monolayers of compounds **1** and **3**. The films were spread at fixed area corresponding to the 45 mN/m surface pressure. Using grazing-incidence geometry and resolving both the surface-normal (q_z) and in-plane (q_r) scattered wave-vector components, two diffraction peaks were observed for each of these compounds on water. The data are shown as functions of q_r integrated for improved statistics over two q_z intervals in Figure 2a for both compounds. A strong peak positioned at $q_r = 1.38$ Å^{-1} for both compounds indicates that a molecular spacing of 4.55 Å exists within the film plane, correlated over ~100 Å length scales. This molecular spacing is in excellent agreement with molecular models of the hydrogen-bonded bis-urea units and also with bulk diffraction data from a related three-dimensional compound.[39] The nonzero q_z component, with a magnitude of 0.30 Å^{-1} for **1** and 0.43 Å^{-1} for **3**, indicates that the molecular form factor is tilted from the surface normal by 12.3° and 17.3° for **1** and **3**, respectively. Such structures are observed when the molecular backbones or alkyl tails are tilted relative to the film plane. A second peak is observed, with $q_r = 1.56$ Å^{-1} for **1** and 1.47 Å^{-1} for **3**, which indicates structural organization with a characteristic in-plane spacing of 4.0 Å in the case of **1** and 4.3 Å in the case of **3**. This clearly suggests a model in which H-bonded molecular units have a spacing in a second direction which depends on head group size. In the case of **1**, the 4.0 Å spacing again agrees with that

(36) This comparison could not be made for **4** due to the rearrangement of the monolayer.
(37) Huo, Q.; Russev, S.; Hasegawa, T.; Nishijo, J.; Umemura, J.; Puccetti, G.; Russell, K. C.; Leblanc, R. M. *J. Am. Chem. Soc.* **2000**, *122*, 7890−7897.
(38) Versteegen, R. M.; Sijbesma, R. P.; Meijer, E. W. *Macromolecules* **2005**, *38*, 3176−3184.
(39) Koevoets, R. A.; Versteegen, R. M.; Kooijman, H.; Spek, A. L.; Sijbesma, R. P.; Meijer, E. W. *J. Am. Chem. Soc.* **2005**, *127*, 2999−3003.

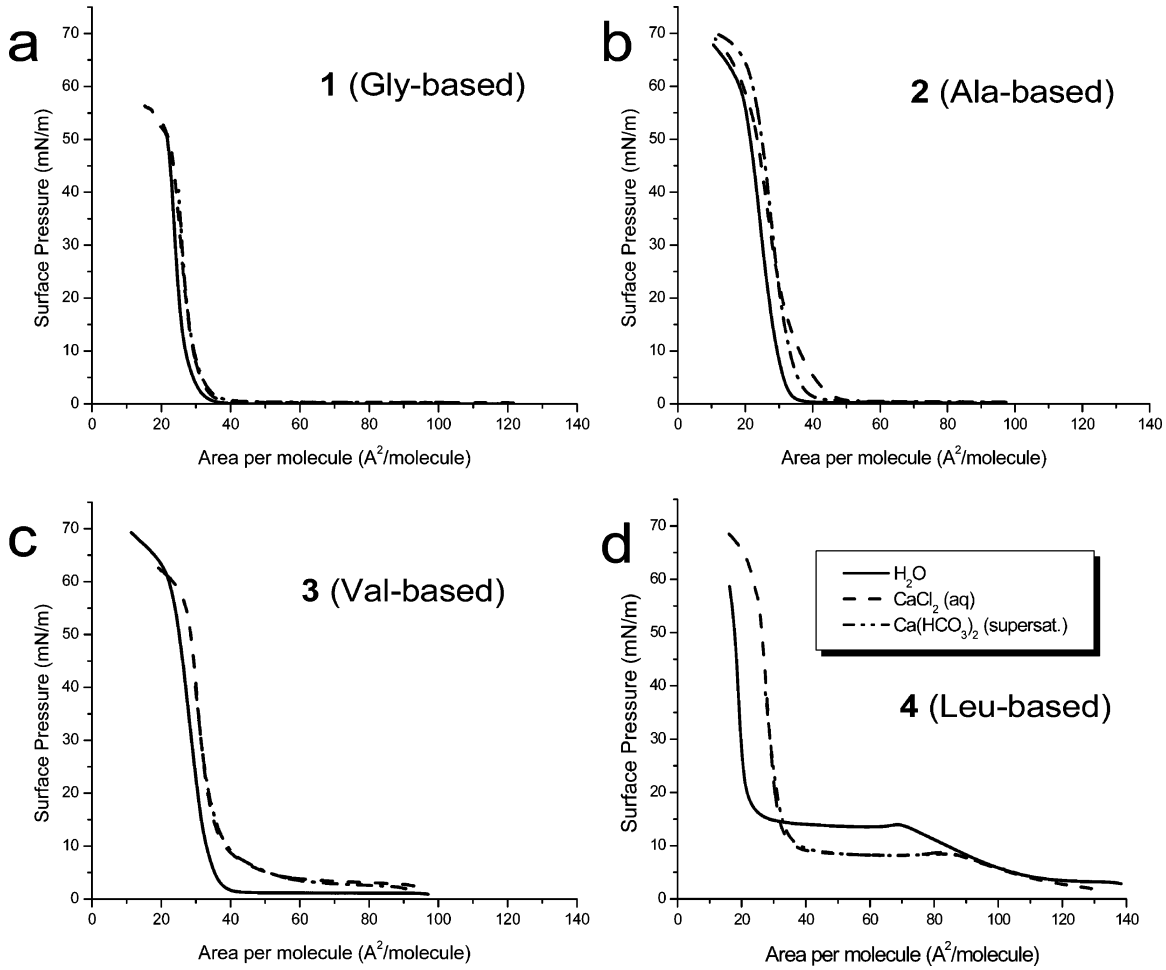

Figure 4. $\pi-A$ isotherms of (a) **1**, (b) **2**, (c) **3**, and (d) **4** on subphases containing water, 9 mM $CaCl_2$, and 9 mM $Ca(HCO_3)_2$.

found in a closely related bis-urea based ammonium surfactant.[40] These second peaks occur at greater q_z values of 0.9 $Å^{-1}$ for **1** and 0.75 $Å^{-1}$ for **3**. Respective molecular tilts of 30.0° and 27.0° are implied.

Additional information about the structures is obtained from X-ray reflectivity measurements of the films, which provide information about the film density along the surface normal. Reflectivity data for the valine based compound **3** on water are shown in Figure 3a. The oscillations derive from constructive interference between the air−film and film−subphase interfaces. We generated a simple two-slab model in which electron density, thickness, and interface roughnesses were free to vary, with no constraints on the parameters (Figure 3b). In this free fit the extracted parameters describe a film of 22 Å thickness and mean molecular area of 37 $Å^2$/molecule. The mean molecular area is in good agreement with Langmuir isotherm data.[41] The measured film thickness is significantly less than the modeled length of the extended molecules, requiring a structure in which the alkyl tails are folded and/or have extreme molecular tilts.

Hence the X-ray measurements provide information about molecular packing, mean molecular area, film thickness, and relationships to the structures of related bulk compounds. Based on these data the following film structure is proposed. Neighboring molecules stand with their bis-urea units hydrogen-bonded to their neighbors, at a spacing of 4.55 Å in the layer plane. The simplest way to model the experimentally determined tilts is to tilt the entire backbone; however, this arrangement disrupts optimal H-bond orientation (Figure 2c). An alternative might be to tilt only the alkyl chains (Figure 2d). Either way, ribbons of H-bonded molecules would be available to assemble next to each other, with some characteristic spacing of 4.0 and 4.3 Å for **1** and **3**, respectively. If assigned to the head group spacing in this orthogonal dimension, these values imply a unit cell area on the order of 19 $Å^2$, which is approximately half the value for the estimated molecular areas as determined from reflectivity and Langmuir isotherms. Instead, the ∼4 Å value matches very well the spacing between close packed alkyl chains. Our observations can be explained if the alkyl tails are folded back between the ribbons, as shown in Figure 2e. This is in good agreement with spacings between alternate rows of backbones and tails of 4.0 Å for **1** and 4.3 Å for **3**, which have similar scattering factors in this configuration. To achieve the required tilt, the entire assembly of ribbons may lean toward

(40) Vos, M. R. J.; Jardí, G. E.; Pallas, A. L.; Breurken, M.; van Asselen, O. L. J.; Bomans, P. H. H.; Leclere, P. E. L. G.; Frederik, P. M.; Nolte, R. J. M.; Sommerdijk, N. A. J. M. *J. Am. Chem. Soc.* **2005**, *127*, 16768−16769.

(41) Although the difference between 37 $Å^2$ from X-ray scattering and 34 $Å^2$ from Langmuir isotherms is on the order of the differences between areas from isotherms of all compounds, somewhat different assumptions are made in the two techniques. The isotherm is performed out of equilibrium, and the extrapolation is made assuming that could the isotherm be performed adiabatically, the intercept would indicate the state where all molecules are optimally spaced. In the reflectivity measurement, the system is in equilibrium and an average density is measured, which reflects nonideal circumstances such as gaps between ordered domains, or the result of losing molecules to the trough edge or subphase, both of which could increase the mean molecular area.

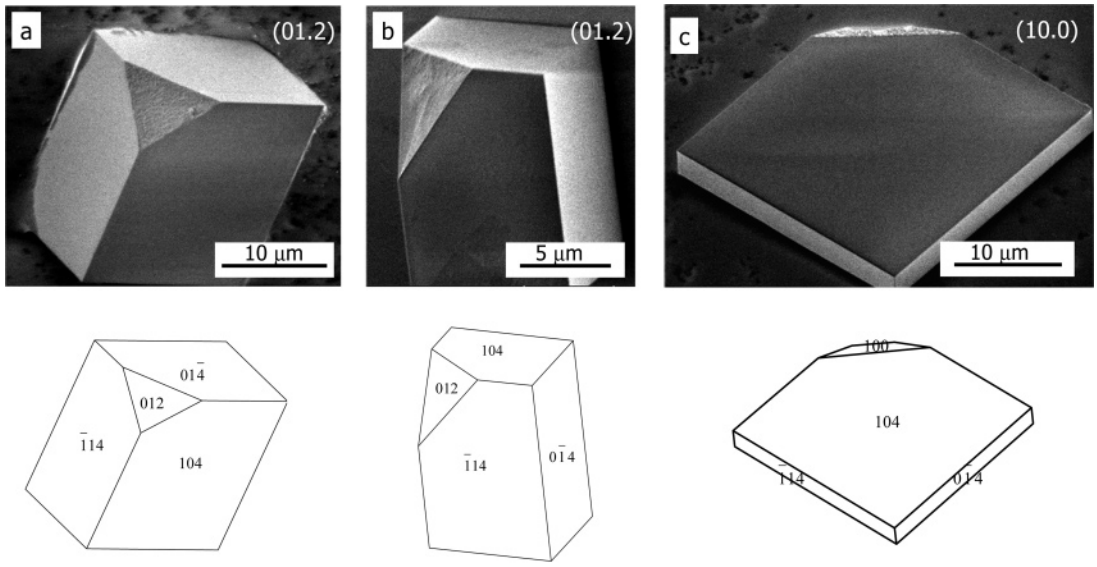

Figure 5. Top: SEM images of (01.2) (a, b) and (10.0) (c) oriented crystals grown under the monolayer of **2** isolated after (a, c) 4 h and (b) 20 h. Bottom: SHAPE[43] models of the crystals shown in (a), (b), and (c), respectively. Crystals viewed from the side that was exposed to the monolayer; the roughened (nucleating) faces have been attached to the monolayer.

the next. This allows space for the two different head group sizes and slides the folded tails lower to interdigitate further between the backbones. The height of this model film is ∼20 Å, close to that computed from free reflectivity fits.

The structure resulting from these considerations explains both the Langmuir isotherms as well as the reflectivity data that give mean molecular areas of 34 Å^2 and 37 Å^2, respectively, and which are derived from completely independent and well-reproduced measurements.[41] It also shows a reasonable agreement with the in-plane diffraction data that suggested the half-sized unit cell dimension of 19.6 Å^2, and thereby a molecular area of ∼39 Å^2. In the ribbon-like aggregates of the related ammonium surfactants these lattice parameters are achieved by packing alternate sheets of molecules upside down, allowing room for head groups while the backbones are interdigitated between them.[40] Here, the ∼20 Å thick film positions the head groups only at the water, as the reflectivity data confirm. At this point we remain puzzled only by the apparent tilt of molecules within the ribbons, which shifts the bonded bis-urea units which should be in registry with each other. The IRRA spectra (not shown) do show a small residual amide I peak for **3**, which has the greater tilt, but not for **1**. Yet, the position of this peak and the amide II bands of both compounds indicate strong H-bonding. Alternatively, if we try to explain the nonzero q_z components of the 4.55 Å peak by tilting just the alkyl tails, the packing of tails between backbones would become untenable. Also, one more Bragg peak with $q_z = 0$ should in this case have been observed, from constructive interference between backbones. Future molecular modeling may help to determine the energetics of other forces such as subphase−head group solvation and alkyl tail packing which stabilize the structure.

At the same time the grazing-incidence X-ray measurements allow us to assess flexibility of the monolayers by recording the response of the film to calcium ions. In-plane diffraction from compound **1** on a $CaCl_2$ subphase (Figure 2b) shows that the peak positions, and hence the molecular spacings, are unchanged. For compound **3** on $CaCl_2$, the H-bonding peak remains unchanged but the secondary peak disappears. Evidently the presence of Ca^{2+} in the subphase interacts sufficiently with the valine head group so as to disrupt film organization, a sign that compound **3** represents a regime in which the film can adapt to the presence of a mineral. Likewise, reflectivity measurements show a distinct increase in electron density at the head group region of compound **3**, due to the presence of associated Ca^{2+} (Figure 3b).

This propensity for Ca-dependent film reorganization was investigated in more detail by $\pi-A$ isotherms from all four compounds on subphases containing 9 mM $CaCl_2$ (Figure 4). For **1** the change in mean molecular area is small (3 Å^2). For **2** the $\pi-A$ isotherm shows a somewhat larger change in mean molecular area from 30 Å^2 to 36 Å^2 indicating some limited potential for adaptation to the presence of calcium ions. In contrast, more significant changes are recorded for **3** and **4** on Ca^{2+}-bearing subphases. In the case of **3** this leads to a small change in the limiting molecular area (from 34 to 37 Å^2) but to a significant change in the lift-off area (from 40 to 70 Å^2). In the case of **4** the lift-off area remained virtually unchanged; however an early onset of the plateau at 90 Å^2/molecule (8 mN/m) as well as of the liquid condensed phase (33 Å^2/molecule) were now observed. Evidently, the larger head groups of **3** and **4**, which prevent tight packing as discussed above, result in more flexible monolayers that can respond to the presence of calcium ions and hence to calcium mineral formation.

Mineralization Experiment. The monolayers of **1**−**4** were used as templates for the crystallization of calcium carbonate. Experiments were carried out by spreading the surfactants on a supersaturated 9 mM $Ca(HCO_3)_2$ solution. The crystallization experiments were performed both by using compressed monolayers, as well as by allowing the surfactants to self-organize on a $Ca(HCO_3)_2$ subphase in crystallization dishes. The crystals were collected from the air−water interface after durations between 7 min and 20 h.

The efficiency of induction differed significantly between the different surfactants. Where glycine derivative **1** was most effective in inducing crystal growth (nucleation density 202 mm^{-2},[42]), this ability decreased going to alanine derivative **2**

(42) See Supporting Information.

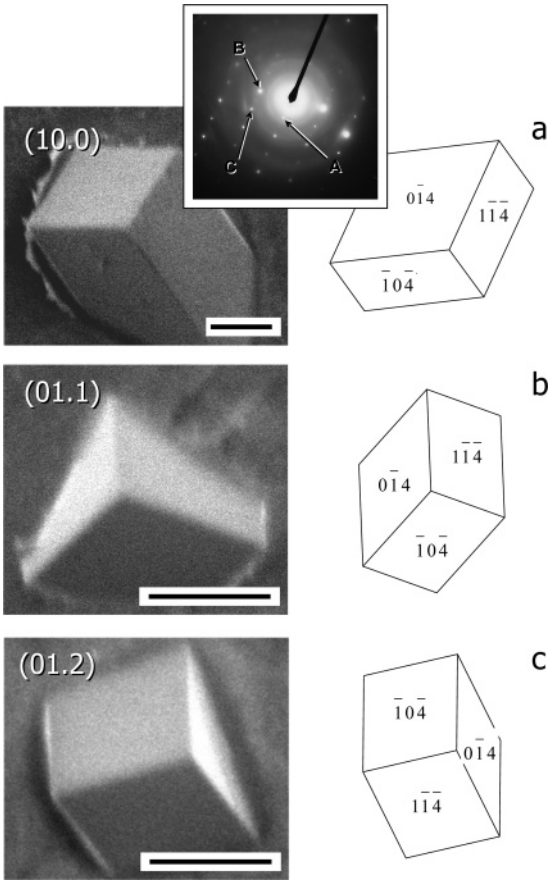

Figure 6. (a) (10.0), (b) (01.1), and (c) (01.2) oriented calcite crystals isolated from beneath a monolayer of **2** on a TEM grid by Langmuir−Schaefer transfer after 15 min. Left: SEM images. Scale bars: 1 μm. Crystals observed from the side exposed to the mineralization solution. Right: SHAPE models[43] of calcite crystals viewed down perpendicular to the corresponding nucleating face: (10.0) (a), (01.1) (b), and (01.2) (c). Inset (a): Electron diffraction pattern corresponding to the [10.0] zone of calcite. Reflections A, $(0\bar{1}.2)$ (3.86 Å); B, $(0\bar{1}.\bar{6})$ (2.38 Å); C, $(02.\bar{4})$ (1.93 Å). Angles, $(0\bar{1}.2)\wedge(0\bar{1}.\bar{6}) = 84°$; $(01.2)\wedge(02.\bar{4}) = 54°$. Camera length: 60 cm.

(104 mm^{-2}), to valine derivative **3** (48 mm^{-2}), and further to the leucine-derived **4** (34 mm^{-2}).

Although the nucleation density was highest using the surfactants with the smaller side groups (**1** and **2**), their ability to stabilize a crystal face other than those of the {10.4} family was lower than for the ones with the larger side groups (**3** and **4**). More precisely, only 15% of the crystals nucleated under monolayers of **1** and **2** showed crystal faces other than {10.4}. For **1** no particular face was dominating in this collection, while for **2** these crystals expressed a new face which according to modeling (using SHAPE[43]) was predominantly oriented parallel to the (01.*l*) plane (with $l = 1-2$) and for a small fraction (<10% of the number of modified crystals) parallel to the (10.0) plane (Figure 5). Within the {01.*l*} type, crystals with a {01.2} orientation were predominant. Electron diffraction analysis of young crystals revealed that after 7 min most of the modified crystals had a {10.0} orientation whereas SEM showed that already after 15 min the ratio {10.0} oriented crystals to {01.*l*} oriented crystals was 1:2, with the {01.2} type becoming dominant in time (Figure 6).

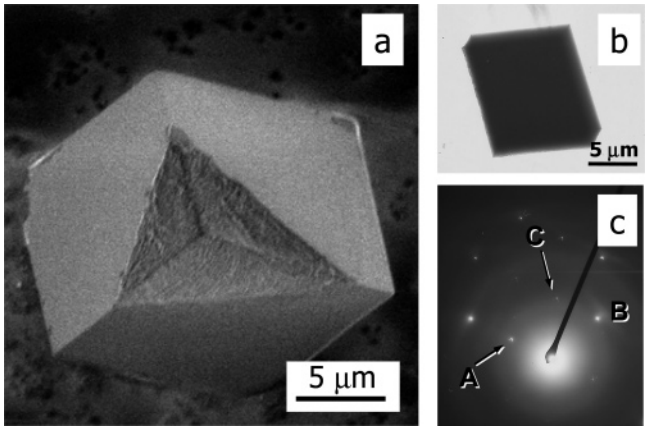

Figure 7. (a) SEM image of modified crystal with a concave indentation isolated from beneath a monolayer of **3** after 4 h. Crystal viewed from the side that was exposed to the monolayer. (b) TEM image of a young crystal isolated after 15 min and (c) its corresponding electron diffraction pattern. The pattern corresponds to the [10.0] zone of calcite. Reflections A, (00.6) (2.84 Å); B, $(02.\bar{3})$ (2.02 Å); C, $(02.\bar{3})$ (2.02 Å). Angles, $(00.6)\wedge(02.\bar{3}) = 111°$; $(00.6)\wedge(02.\bar{3}) = 69°$. Camera length: 60 cm.

Although no specific habit modification was observed for **1** the high nucleation density was attributed to the presence of carboxylate groups at the template surface. This was confirmed by comparing the activity in calcium carbonate nucleation with oligoethylene derivative **5**. This nonionic bis-urea surfactant also forms close packed Langmuir monolayers with a similar density (MMA 25 Å^2, lift-off area 39 Å^2/molecule) and also gives rise to the formation of randomly oriented {10.4} calcite, however, with a much lower nucleation density (18 mm^{-2}).

In contrast, surfactants **3** and **4** led to the formation of significant proportions of crystals that were different from rhombohedral {10.4} calcite. When a monolayer of **3** was used, again all crystals were calcite of which ~70% were characterized by a concave indentation defined by three roughened planes.[20] Selective area electron diffraction performed on young crystals, isolated after 15 min from the beginning of the experiment, revealed that these early crystals all had a {10.0} orientation, suggesting that the crystals had nucleated from this face (Figure 7).

For leucine-derivative **4** the results of the mineralization study reflected the different self-assembling behavior of this surfactant. Here the formation of populations of predominantly calcite and of predominantly aragonite under separate areas of the monolayer was observed, which suggested the presence of domains with different degrees of order. Significantly, the observed calcite crystals were small (5−10 μm) compared to those formed under a monolayer of **3**. This suggests that calcite nucleates in a later stage than aragonite. It was speculated that this may be due to the more bulky side group of leucine that slows down the self-organization of the surfactants. Indeed at earlier time points (15 min) the collected crystals consisted mainly of aragonite, now together with a small amount of vaterite. This supports the suggestion that a lower degree of organization of **4**, as present in the earlier stages of the process, promotes the formation of aragonite over calcite (Figure 8). Similar observations were made by Küther et al. who related the induction of aragonite formation to the disorder in self-assembled monolayers

(43) Calcite crystals were modeled with *SHAPE* V7.1.2; Shape Software: Kingsport, TN, U.S.A., 2004.

(44) Küther, J.; Nelles, G.; Seshadri, R.; Schaub, M.; Butt, H.-J.; Tremel, W. *Chem.—Eur. J.* **1998**, *4*, 1834−1842.

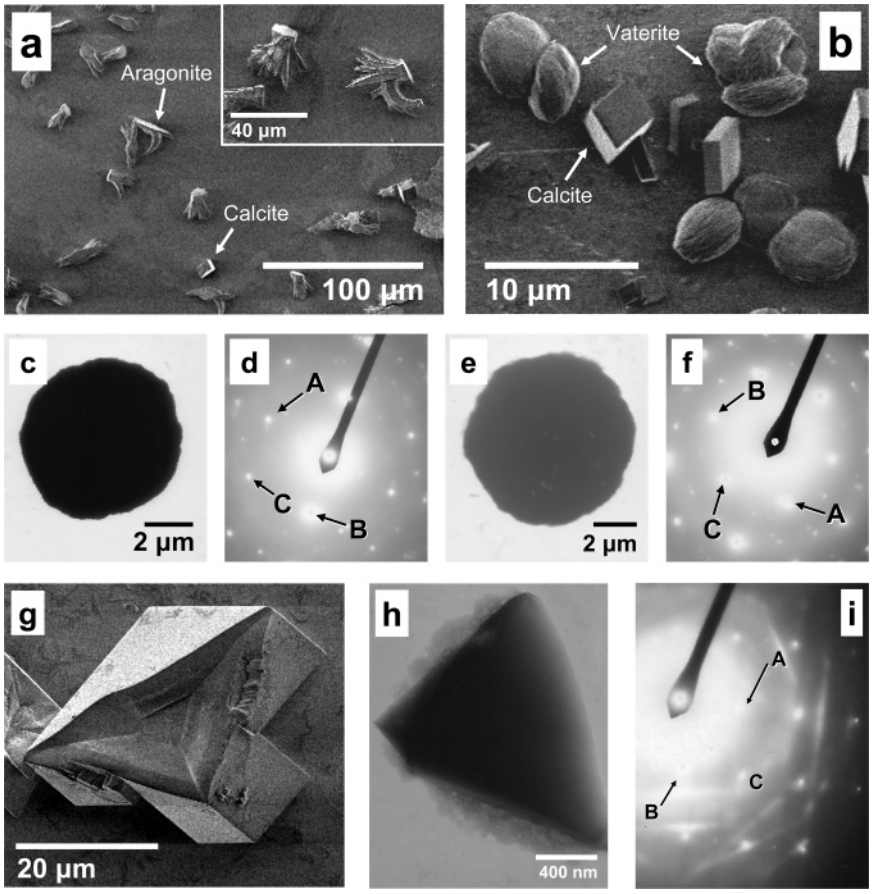

Figure 8. SEM images of crystals isolated from under a noncompressed monolayer of **4** after 4 h (a) and 15 min (b). The inset in (a) shows a magnification of the aragonite crystals in (a). (c) TEM image of a young crystal isolated after 15 min under a noncompressed monolayer of **4** and (d) its corresponding electron diffraction pattern. The pattern corresponds to the $[\bar{1}2.\bar{3}]$ zone of aragonite. Reflections A, (12.1) (2.73 Å); B, $(\bar{1}\bar{1}.\bar{1})$ (3.40 Å); C, (21.0) (2.37 Å). Angles (12.1)∧$(\bar{1}\bar{1}.1)$ = 101°; (12.1)∧(21.0) = 43°. Camera length: 60 cm. (e) TEM image of a young crystal isolated after 15 min under a noncompressed monolayer of **4** and (f) its corresponding electron diffraction pattern. The pattern corresponds to the [00.1] zone of vaterite. Reflections A, (10.0) (3.76 Å); B, $(0\bar{1}.0)$ (3.76 Å); C, $(1\bar{1}.0)$ (3.76 Å). Angles (10.0)∧$(0\bar{1}.0)$ = 120°; (10.0)∧$(1\bar{1}.0)$ = 60°. Camera length: 60 cm. (g) Modified calcite crystal with an indented truncated face, isolated from under a compressed monolayer of **4** after 4 h. Crystal viewed from the side that was exposed to the monolayer. (h) TEM image of a young crystal isolated after 15 min under a compressed monolayer of **4** and (i) its corresponding electron diffraction pattern. The pattern corresponds to the [10.0] zone of calcite. Reflections A, (01.6) (2.38 Å); B, $(02.\bar{3})$ (2.02 Å); C, (03.3) (1.40 Å). Angles (01.6)∧$(02.\bar{3})$ = 78°; (01.5)∧(03.3) = 42°. Camera length: 30 cm.

on gold colloids.[24,26,44] Growing calcium carbonate under a compressed monolayer of **4** resulted in the formation of predominantly calcite, implying that in the mineralization dishes the calcite was indeed formed under the more ordered domains. However, it should be noted that for **4** the compressed film may comprise a double layer, rather than a monolayer, as discussed above.

The majority (>70%) of the calcite crystals grown under monolayers of **4** was habit modified showing an often indented, truncated face at one of the corners of the rhombohedral form. The indentations of the crystals resembled those observed for **3** but were less regular in shape. Selected area electron diffraction on early crystals that were collected by Langmuir−Schaefer transfer from under the compressed monolayer indicated that also these were nucleated from the (10.0) plane.

Adaptability of the Template. To investigate in more detail how the effectiveness of these surfactants to induce oriented nucleation relates to their ability to reorganize to the demands of the new crystal face, we compared the $\pi-A$ isotherms of **1**−**4** both on subphases containing 9 mM $CaCl_2$ and on subphases containing 9 mM $Ca(HCO_3)_2$.[21] For **1** the $\pi-A$ isotherms only showed small changes going from $CaCl_2$ to $Ca(HCO_3)_2$ containing subphases. For **2** it is interesting to note that the molecular area increase is larger between water and $CaCl_2$, going from 30 to 36 Å^2, than that from water to the mineralizing $Ca(HCO_3)_2$ subphase, going from 30 to 34 Å^2. This limited ability of **2** to adapt to the growing mineral phase is in line with the results of the mineralization experiments. Apparently the molecular organization of **2** changes to some extent on the $Ca(HCO_3)_2$ containing subphase, but at a slow rate leading to the nucleation of different types of habit modified crystals at different points in time. For **3** and **4** no differences were observed between the isotherms of the two different Ca^{2+} containing subphases. These results suggest that these more flexible monolayers respond to the presence of calcium ions in a way which makes them immediately suitable for the nucleation of {10.0} modified calcite.

Considerations on the Mechanism of Crystal Formation. As for surfactants **2** and **4** the types of crystals produced, as well as the molecular organization of the template, changed in the course of the crystallization experiments, it was not possible to identify a specific relation between the organic and inorganic phase for these two compounds. In contrast, for surfactant **3** only one type of crystal habit modification was observed. Nevertheless, the limiting MMA on aqueous $CaCl_2$ (37 Å^2) observed for **3** has only an approximate relation to the cation

Chart 1

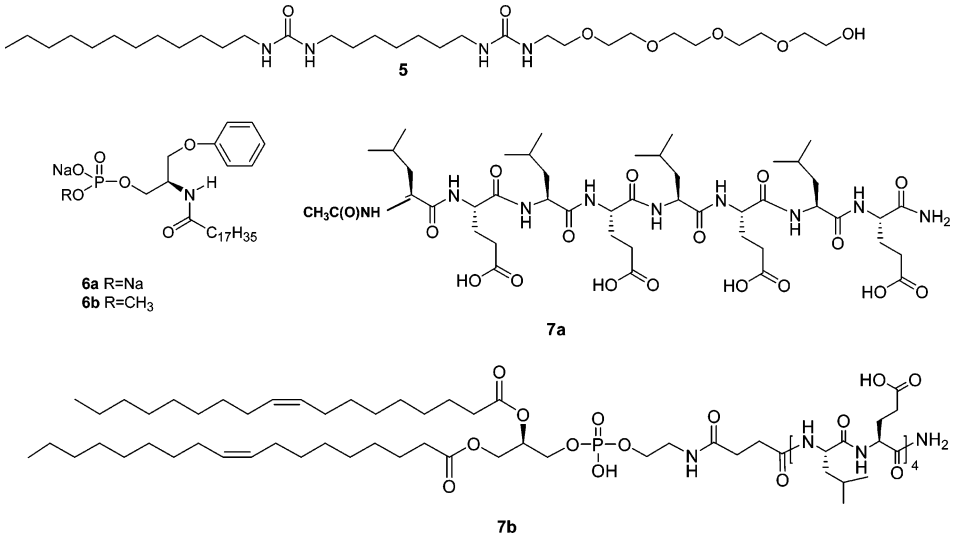

lattice parameters ($a = 4.99$ Å, $b = 8.53$ Å) in the (10.0) face of calcite, and there was no evident match of any *d*-spacing in the X-ray data. It is important to note that the formation of {10.0} calcite is not very common.[45−50] Nevertheless we have reported on its formation already on two earlier occasions. Although in both cases the templates were Langmuir monolayers, the molecules that were used were quite dissimilar, ranging from amide-containing phospholipids[18] (**6a**,**b**) and β-sheet forming amphiphilic peptides[21] (**7a**,**b**) to the present bis-urea based amino acid amphiphiles (Chart 1). Also in these cases no obvious relation between the average molecular area and the lattice parameters of the nucleating {10.0} phase could be deduced.

Following the suggestion of Volkmer et al.[29] that the oriented nucleation of calcium carbonate is governed by the distribution of electrostatic interactions, we calculated the charge density of the monolayer of **3** to be 2.7. This number however does not agree very well with the charge densities of 1.8−2.0 $e^{-}\cdot nm^{-2}$ that can be calculated for **6** and **7** and hence does not explain the present observations.[18,21] However, a common feature present in all templates is the fact that they interacted with the aqueous phase either through a carboxylic acid group or by a bidentate-type orientation of two of the oxygen atoms of a conformationally restricted phosphate group. Although it is has been demonstrated repeatedly that there is no need for an epitaxial relation between the template molecules and the nucleating face, it is interesting to note that in these cases mentioned the 2D organization of the functional groups has a dominating repeating distance of 4.5−5 Å that is dictated by the formation of hydrogen bonds.

In the present study this is emphasized by the partial disruption of the organization of the monolayer of **3** upon exposure to calcium ions leaving only the repeating distance of bis-urea hydrogen bonds. Moreover in the case of both **2** and **7a** the limited ability of the template to adapt to the developing inorganic phase seems to favor the formation of calcite nucleated from one of the {01.*l*} faces, while the more adaptable templates (**3**, **4**, **6**, **7b**) trigger the nucleation of the {10.0} face.

Conclusion

A new system of bis-urea based surfactants containing amino acid head groups has been prepared and used to form self-organizing monolayers that induce the formation of $CaCO_3$. We have shown that by the choice of the amino acid we can systematically alter the density of the surfactant molecules in a monolayer and their ability to respond to the presence of calcium ions. Whereas the surfactants based on glycine, alanine, and valine formed stable monolayers that could be compressed to high surface pressures before a collapse was observed, the leucine based surfactant rearranged to form more than one layer already at low surface pressures. Nevertheless, within the series an increase in the amino acid side groups appears to correspond with the ability to induce the nucleation of unusual crystal planes.

The glycine and alanine based surfactants form very rigid monolayers that are active in promoting the nucleation of calcium carbonate; however for both compounds this leads to predominantly {10.4} calcite. Whereas no particular nucleation plane was favored in the case of the glycine derived surfactant, in the case of the slightly more flexible alanine based surfactant the majority of the modified crystals belonged to the {01.*l*} family with $l = 1-2$. In contrast, the valine and leucine based surfactants form more flexible monolayers that reorganize their structure upon complexation of calcium ions. Although in the latter two cases we observed a relatively low nucleation density, a high selectivity for the nucleation of {10.0} calcite was found. The glycine and valine derived surfactants were considered to represent a rigid, persistent and a flexible, adapting template, respectively. X-ray measurements not only confirmed the persistence of the bis-urea hydrogen bonds upon exposure to calcium ions but also showed that whereas the glycine based compound maintained its structure, the valine based surfactant released its 2D organization under these conditions.

(45) Mann, S.; Didymus, J. M.; Sanderson, N. P.; Heywood, B. R.; Aso, Samper, E. J. *J. Chem. Soc., Faraday Trans.* **1990**, *86*, 1873−1880.
(46) Archibald, D. D.; Qadri, S. B.; Gaber, B. P. *Langmuir* **1996**, *12*, 538−546.
(47) Walker, J. B. A.; Heywood, B. R.; Mann, S. *J. Mater. Chem.* **1991**, *1*, 889−890.
(48) Rajam, S.; Heywood, B. R.; Walker, J. B. A.; Mann, S.; Davey, R. J.; Birchall, J. D. *J. Chem. Soc., Faraday Trans.* **1991**, *87*, 727−734.
(49) Mann, S.; Heywood, B. R.; Rajam, S.; Walker, J. B. A. *J. Phys. D: Appl. Phys.* **1991**, *24*, 154−164.
(50) Didymus, J. M.; Oliver, P.; Mann, S.; DeVries, A. L.; Hauschka, P. V.; Westbroek, P. *J. Chem. Soc., Faraday Trans.* **1993**, *89*, 2891−2900.

This finding is one of many arguing against a lattice match between the template and the nucleation plane. Also comparison of the charge density of this monolayer with that of others known to induce the formation of {10.0} calcite gives inconsistent values and hence does not allow us to explain our results solely in terms of electrostatic interactions. Although the adaptability of the templating molecules clearly is an important factor in the outcome of the mineralization experiments, the repeated finding of {10.0} oriented calcite when hydrogen bond directed templates are used presently remains unsolved.

Acknowledgment. This research was supported by The Netherlands Scientific Organization (NWO). The authors are grateful to E. W. Meijer for stimulating discussions. B.N.L. is supported by U.S. DOE Contract DE-AC02-98CH10886.

Note Added after ASAP Publication: Reference errors were present in the version published on the Web October 18, 2007. The final Web version published on October 20, 2007 and the print version are correct.

Supporting Information Available: Characterization of compounds **1**−**4** and SEM images. This material is available free of charge via the Internet at http://pubs.acs.

JA075875T